PAPER H

RELATIONSHIPS BETWEEN MATERIAL PROPERTIES AND ANGLE-DEPENDENT REFLECTIVITY

Steven R. Bacharach

ABSTRACT

An elastic wave incident on an interface between two solid half-spaces produces reflected and transmitted waves with amplitudes dependent upon the solids' properties and the angle of incidence and amplitude of the incident wave. Reflectivity is defined as the ratio of the amplitude of a reflected wave to that of the incident wave. *P*-wave to *P*-wave reflectivities (*PP*) obtained from high incident angles are often used to estimate lower half-space compressional velocity by a process known as CDP trace stacking. For this process, it is assumed that using reflectivity values averaged from large incidence angles in the place of the reflectivity value at normal incidence will result in little error in the velocity estimation. Because several variables simultaneously determine reflectivity, analyzing the effect on reflectivity of changing a single one is difficult. However, assuming that the density and the ratio of *S*-wave velocity to *P*-wave velocity are the same in both media, I plot the change of two different ratios of velocity against each other to outline regions corresponding to material properties in which this CDP velocity inversion will be successful to within 5%. If the average reflectivity is approximately equal to the value for normal incidence or near to zero itself, then one can invert for velocity in the lower half-space with little error if densities and upper half-space *P*-wave velocity are known. Assuming constant density across the interface leads, in some cases, to a better velocity inversion; in others inversion is less accurate. So, the accuracy of accounting for density differences is ambiguous.

A compressional wave incident on a solid from a liquid yields, in general, a reflected *P*-wave, a transmitted *P*-wave, and a transmitted *S*-wave. While discrete *PP* values provide little information toward inferring solid properties, an examination of the relationship between the solid's shear velocity and that pre-critical incident angle that yields the maximum *PP* is useful and has possible applications in the field of non-destructive testing. The ratio of the solid density to the liquid density, appears to have little bearing on the relationship between the ratio of shear velocity in the solid and

An elastic wave striking the interface between a solid half-space and a vacuum is a much easier problem to model than the two previous cases. The vacuum has no density and cannot propagate any waves. Therefore, wave reflectivity at the boundary depends only on the ratio of elastic velocities within the solid and the angle which the incident wave makes with the interface. This simplification yields a functional relationship between the velocity ratio in the solid and the angle of incidence, if non-converted wave reflectivity equals zero. This relationship might be useful as a check on sonic log measurements or as a qualitative measurement of isotropy, homogeneity, or elasticity.

For the three previous cases, solid-solid, liquid/solid, and vacuum/solid, I make several assumptions. I calculate reflectivity from equations describing elastic wave propagation and boundary conditions at elastic interfaces and only examine pre-critical incident angles. Also, amplitudes, and therefore reflectivity coefficients, are measured in the direction of wave propagation. So, a geophone, situated above the reflector and measuring a single component of displacement, would have to be corrected according to which component of displacement, horizontal or vertical, it is measuring. Below the reflector, the geophone measurement, after the geometric correction, would be the negative of the value calculated from the equations I use. Another assumption is that all incident and scattered waves are in a plane perpendicular to the interface and are time-harmonic dependent. I also examine only homogeneous waves, such that the phase and energy velocities are equal in direction and magnitude. By relaxing the restrictions on the wave and interface types by looking at inhomogeneous waves interacting with viscoelastic interfaces, several differences from elastic theory appear. Seismic velocities and the quality factor, Q, depend on frequency; phase velocity travels in a different direction than energy velocity, dependent on incident angle

SOLID-SOLID INTERFACE

At the boundary between two solid half-spaces, a *P*-wave, in general, yields a reflected *P*-wave, a transmitted *P*-wave, a reflected *SV*-wave, and a transmitted *SV*-wave [Aki and Richards 1980] (Figure 1). This simple two-layer model is analogous to surface seismic and crosswell survey geometries. Waves are generated at the surface with receivers placed at different offsets (angles) in the former case; in the latter situation, shots and receivers are both downhole, and incidence angle changes according to their vertical locations within the well and the depth of the reflector. These waves'

shots and receivers are both downhole, and incidence angle changes according to their vertical locations within the well and the depth of the reflector. These waves' propagation directions are described by Snell's Law and amplitudes by the Zoeppritz equations. The reflectivity of this interface is the amplitude of a reflected wave divided by that of the incident wave. The reflectivity varies according to the angle of incidence of the wave and the densities and elastic wave velocities of the half-spaces (See Appendix A). The reflectivity from an incident *P*-wave reflecting a *P*-wave is known as *PP*.

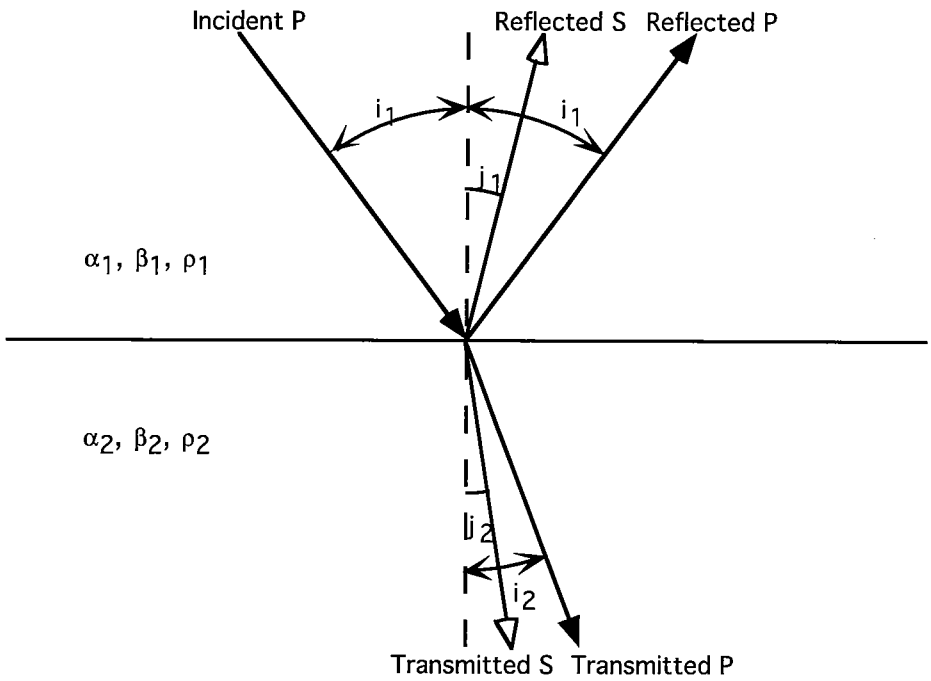

Figure 1: Reflection, transmission, and conversion of a *P*-wave incident on a solid-solid interface. α, β, and ρ are compressional velocity, shear velocity and density, respectively ($\alpha_1 > \alpha_2$) [Tooley *et al.* 1965].

Velocity Inversion from PP Reflectivity and CDP Stacking

Much of the velocity inversion performed today is based on common depth point (CDP) stacking. Shots and receivers are placed at successive intervals along the surface to record the traces of several waves' bouncing off a single reflector point (Figure 2).

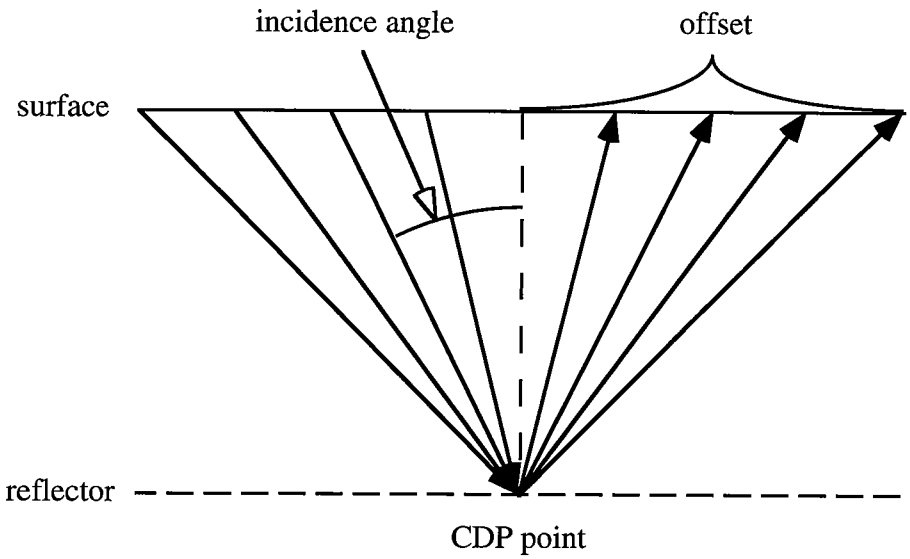

Figure 2: A surface seismic CDP survey - rays emanate from shots on the surface on the left and are reflected to receivers at the surface on the right.

Using an NMO correction, individual traces are moved up to equalize the different pathlengths the waves took to generate them (Figure 3). Traces are then collapsed horizontally to a point on the surface directly above the CDP in a process known as trace stacking.

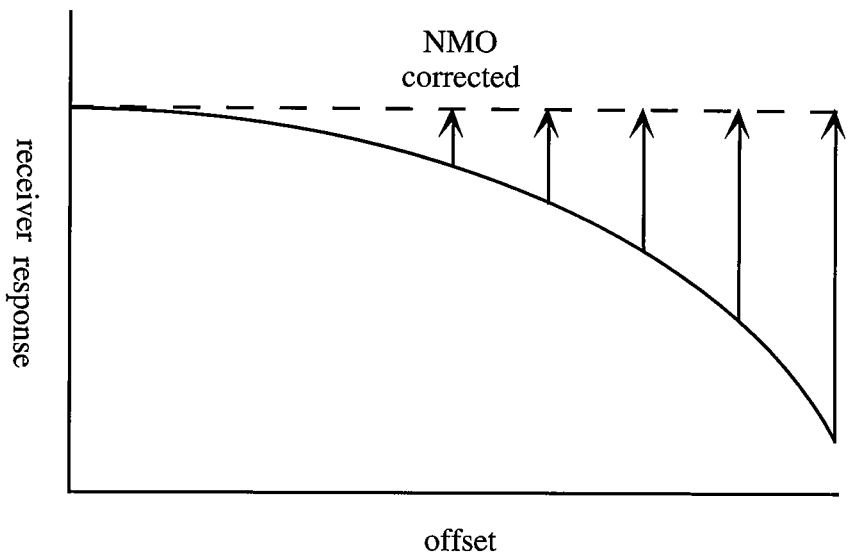

Figure 3: A normal moveout correction adjusts the traces from far offsets according to the distance the ray traveled that created that trace. In this way, traces from nonnormal angles of incidence are used to image a reflector point.

Reflectivity values from nonnormal incident angles are averaged in the stacking process and used as an approximation for *PP* at zero incidence. To study the validity of this approximation, I try to develop relationships between average reflectivity and material properties. Later, I will show that *PP* reflectivities averaged in this way from high angles of incidence will not invert correctly for lower layer compressional velocity, except under certain conditions. Therefore, some of the simple velocity inversion work practiced today, which does not treat reflectivity at nonnormal incidence in a rigorous fashion, is imprecise.

Effect on Reflectivity of Varying a Single Variable

In figures to follow I use velocity and density ratios from a synthetic shale/sandstone contact [Turcotte and Schubert 1982] and from McElroy well logs (West Texas carbonate) at approximately 2845 ft. depth. These ratios are derived from the following velocities and densities:

Synthetic (control): shale - density = 2.60 g/cm3 $\alpha = 4.08$ km/s $\beta = 2.45$ km/s
sand - density = 2.42 g/cm3 $\alpha = 4.12$ km/s $\beta = 2.54$ km/s

McElroy well logs: upper - density = 2.85 g/cm^3 $\alpha = 6.20$ km/s $\beta = 3.55$ km/s
lower - density = 2.71 g/cm^3 $\alpha = 5.84$ km/s $\beta = 3.27$ km/s

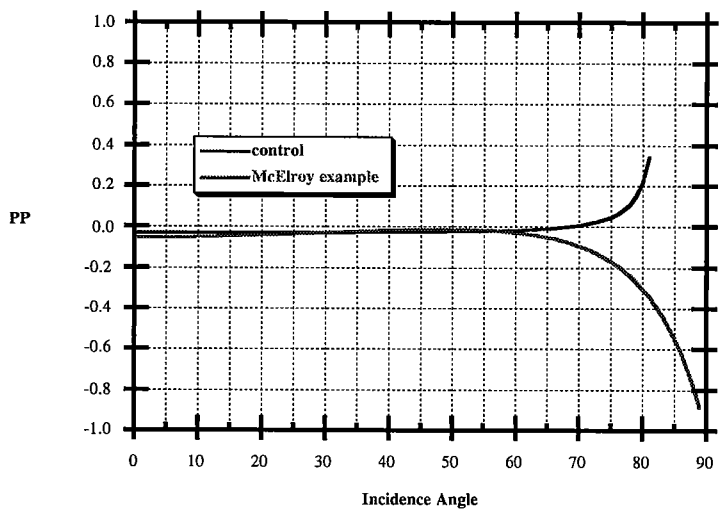

Figure 4: *PP* reflectivity versus angle from the shale overlying sandstone contact and from an interface within the McElroy field. The control curve does not reach 90 degrees, because a critical angle exists at about 81 degrees for this case.

In field seismic surveys, reflectivity is often measured as an average over a range of angles. For surface seismic geometries this range is approximately 0 to 50 degrees, while for crosswell it is approximately 20 to 70 degrees. If the average *PP* does not change appreciably over a wide range of angles, then one can use the value at higher incidence as an estimate for *PP* at normal incidence. Now, at normal incidence the equation for *PP* is much less complicated than the general Zoeppritz equation, because there are no converted waves [Levin 1986]. Assuming constant density, this simplification leads to an inversion scheme for velocity in the lower half-space, given the velocity in the upper half-space and the reflectivity at the interface.

Average Reflectivity

Because reflectivity equations are ratios of a scattered ray property to an incident ray property, they are unitless. Therefore, absolute values for material densities or velocities are meaningless, while using ratios of these values as inputs to the equations is simpler and easier to interpret. I name these input ratios as follows:

$$a=\frac{\alpha_2}{\alpha_1}, \qquad b=\frac{\beta_1}{\alpha_1}, \qquad c=\frac{\beta_2}{\alpha_1}, \qquad r=\frac{\rho_2}{\rho_1}. \tag{1}$$

Using the properties from the synthetic shale/sandstone contact, I vary the separate velocity and density ratios to examine the individual effect each one has on the *PP* reflectivity averaged over a 50 degree window (Figures 5-8). I also examine the average reflectivity data calculated from the McElroy field logs (Figure 9).

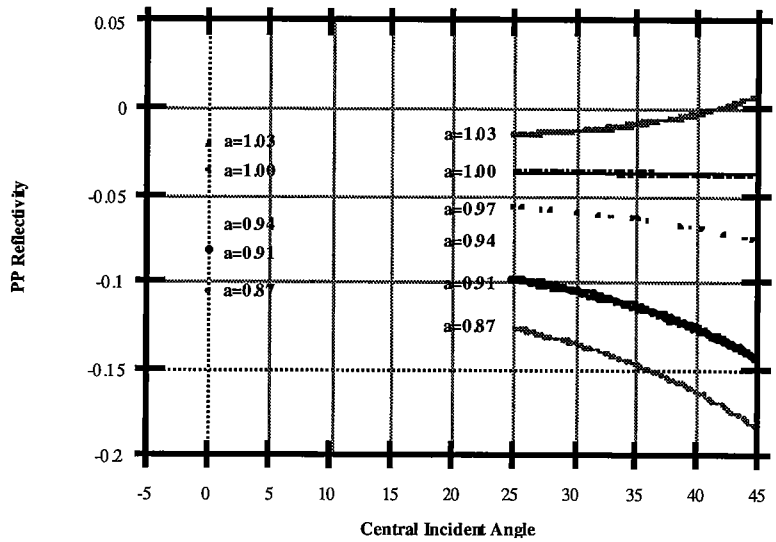

Figure 5: *PP* averaged over a 50 degree window, varying only the *a* ratio. Normal incidence values are dependent on *a* and so are shown to the left of the majority of data points. (shale/sandstone contact: $b = .600$; $c = .623$; $r = .931$)

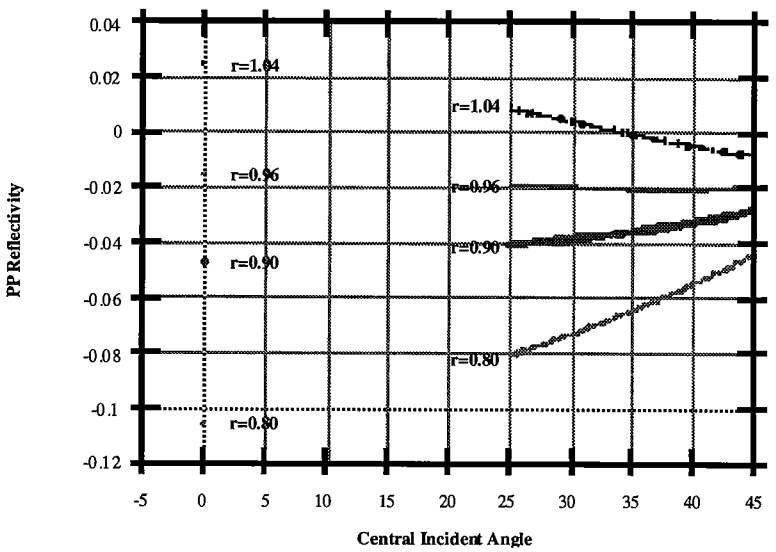

Figure 6: *PP* averaged over a 50 degree window, varying only the *r* ratio. Normal incidence values are dependent on *r* and are shown to the left of the majority of data points. (shale/sandstone contact: $a = 1.010$; $b = .600$; $c = .623$)

In Figure 5, as the range of angles over which *PP* is averaged increases, that average diverges for the different values of *a*, α_2. At the surface seismic end, central incident angle of 25 degrees, only four values of *a*, 0.94, 0.97, 1.00, and 1.03, are close enough to

their respective normal incidence values to be considered candidates for velocity inversion. At the crosswell end, central incident angle of 45 degrees, only the values 1.00 and 1.03 are near enough.

The opposite effect is seen in Figure 6 as central incident angle increases. Now, the average *PP* converges for different density ratios. This effect makes sense since velocity and density have reciprocal effects in the reflectivity equations.

Both Figures 5 and 6 show that normal incidence reflectivity can change sign even if the compressional velocity ratio, *a*, and the density ratio, *r* , do not cross unity. This makes sense because the important quantity determining reflectivity is not either of these values alone, but the impedance, the product of velocity and density. Normal incidence reflectivity in terms of impedance is:

$$PP = \frac{Z_2 - Z_1}{Z_2 + Z_1} . \qquad (2)$$

If the impedances are replaced by the corresponding velocity and density ratios, then

$$PP = \frac{\mathbf{ar} - 1}{\mathbf{ar} + 1} . \qquad (3)$$

Figures 7 and 8 illustrate changes in average *PP* due to changing the *b* and *c* ratios, the shear velocity values. In these cases, both graphs diverge toward higher angles, so velocity inversion for crosswell geometries would be less likely than for surface seismic ones. However, as *b*, or β_1, increases, reflectivity goes up, whereas a similar increase in β_2 causes reflectivity to drop.

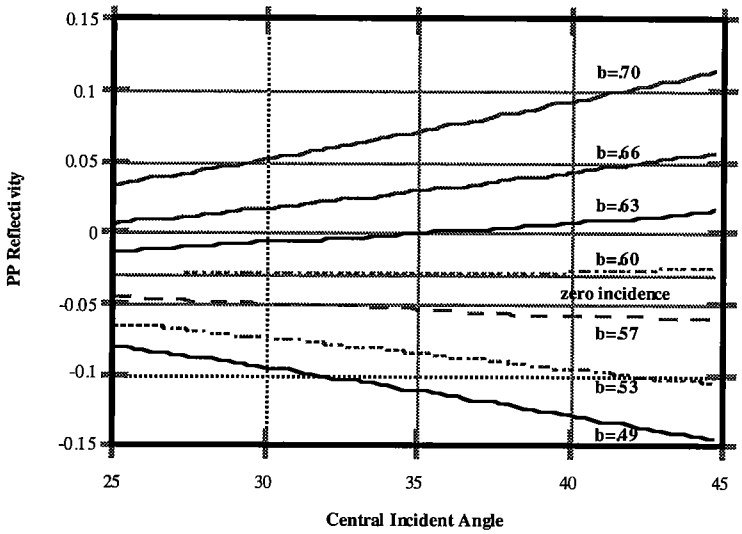

Figure 7: *PP* averaged over a 50 degree window, varying only the *b* ratio. Normal incidence is flat because it is independent of *b*. (shale/sandstone contact: a = 1.010; c = .623; r = .931)

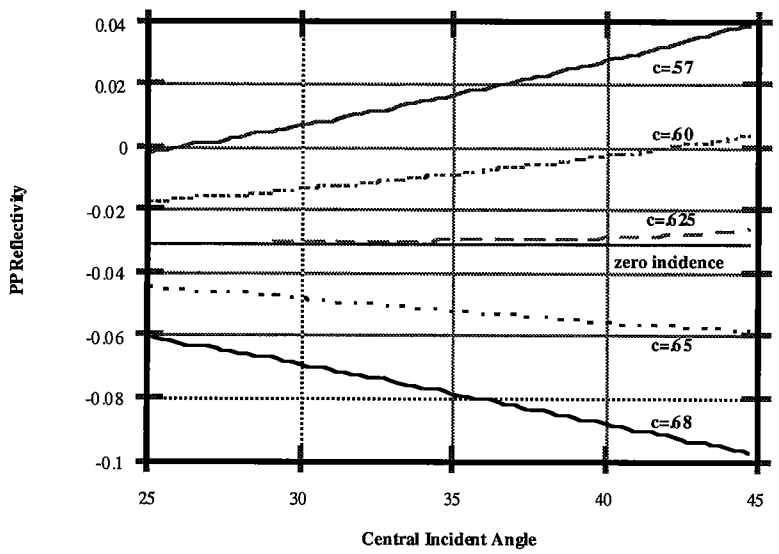

Figure 8: *PP* averaged over a 50 degree window, varying only the *c* ratio. Normal incidence is flat because it is independent of *c* . (shale/sandstone contact: a = 1.010; b = .600; r = .931)

Figure 9 indicates that differences between the McElroy angular average and the McElroy normal incidence seem much too great (> 50%) for velocity inversion to be feasible according to this single ratio analysis. However, as will be shown later, McElroy log numbers do invert very accurately for lower compressional velocity. Accounting for

density and *P*-wave velocity differences simultaneously leads to better velocity estimates. Also, because the absolute values of normal incidence and averaged *PP* are both near zero, reflectivity is "damped" in the formula for α_2.

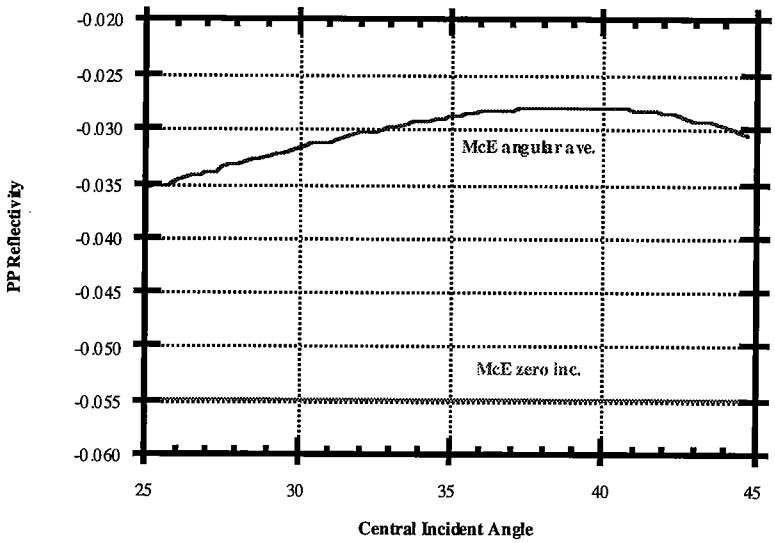

Figure 9: *PP* averaged over a 50 degree window using ratios from a McElroy log. McE zero inc. is the McElroy reflectivity at normal incidence.

The individual velocity and density ratios are too coupled within the Zoeppritz equations, making the interpretation of changing a single ratio meaningless. In fact, the equation for the calculation of PP involves so many factors that the only meaningful assumption resulting in a significant simplification is normal incidence. Other assumptions, such as constant density and Poisson solids, $\alpha/\beta = (3)^{1/2}$, are not sufficient to obtain a simple relationship for velocity ratios as a function of incidence angle.

Using smaller angular windows does not help to constrain the variability of average *PP* with respect to angle. In fact, smaller windows yield average *PP* values that vary more, because they are smoothed from fewer angles. Larger windows could make average *PP* curves slightly flatter, but windows much larger than 50 degrees in the field are rare, and would not flatten average *PP* curves significantly anyway.

I also examine *PP* averages using my control numbers and the McElroy numbers over different angular ranges from zero degrees (Figure 10). Unfortunately, the following figure does not indicate that either case exhibits behavior in a regular pattern that could lead to an inversion scheme.

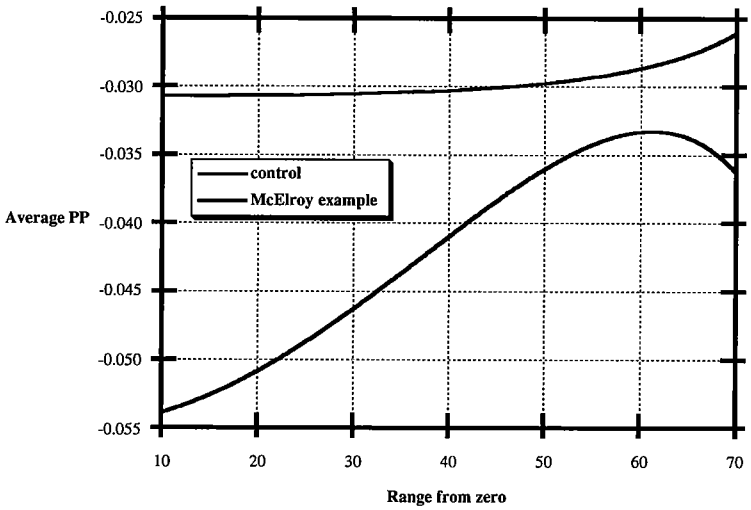

Figure 10: *PP* reflectivity averaged over increasing angular ranges beginning at normal incidence and ending at the angle indicated on the horizontal axis.

A single variable study of the effect on reflectivity, averaged over a moving 50 degree window or a lengthening window starting at normal incidence, is not very enlightening. A two or three ratio model is more appropriate to delineate the range of velocity ratios such that the average angular *PP* remains within a certain tolerance level compared to normal incidence reflectivity *PP* (Figure 11).

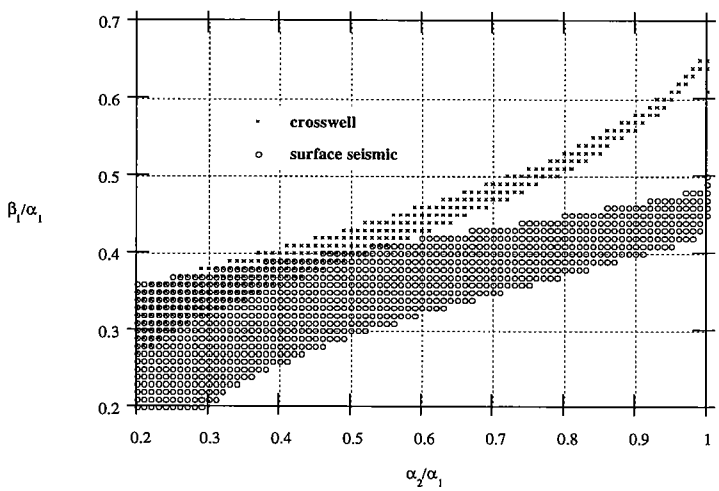

Figure 11: Shaded areas show values of β_1/α_1 and α_2/α_1 such that the average angular *PP* and normal incidence *PP* differ by less than 5% (crosswell is averaged from 20 to 70 degrees; surface seismic is averaged from 0 to 50 degrees).

Velocity Inversion

Inputting the *PP* value averaged from higher angles into the formula for reflectivity perpendicular to the boundary, I can solve for compressional velocity in the lower medium analytically:

$$PP(i=0°)=\frac{\rho_2\alpha_2-\rho_1\alpha_1}{\rho_2\alpha_2+\rho_1\alpha_1}, \tag{4}$$

where i is angle of incidence, can be solved for α_2 if we assume that $\rho_1=\rho_2$. This assumption yields:

$$\alpha_2=-\alpha_1\left(\frac{PP+1}{PP-1}\right). \tag{5}$$

I use two different methods to make envelopes of error in the estimation of α_2. First, I directly compare α_2 using the average angular *PP* in Eqn. (5) to the original value. The second method is a mathematical construction in which I introduce a small error into the estimate of *PP* and deduce the size of the resulting error in α_2 (Appendix B). The following two error envelopes are designed using two constraints. I assume, as in Eqn. (5), that r = 1. Also, to simplify the problem to two variables from three, I assume that $(\beta_1/\alpha_1) = (\beta_2/\alpha_2)$, or $c = a \times b$.

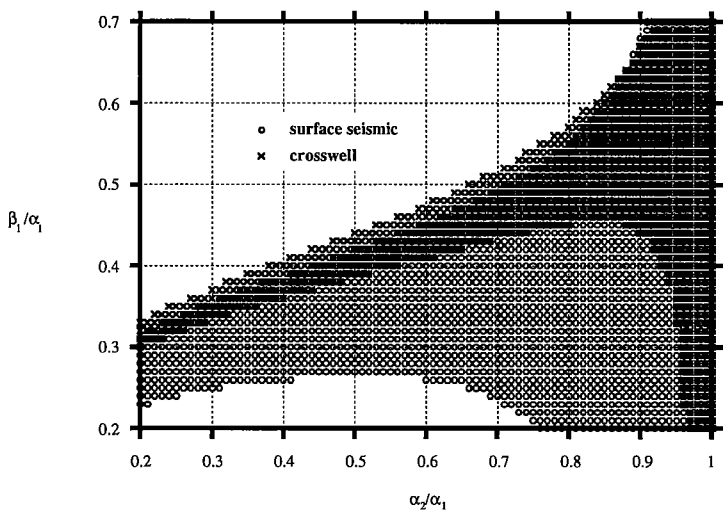

Figure 12: Shaded areas denote values of β_1/α_1 and α_2/α_1 such that α_2 estimated from average angular *PP* and actual α_2 differ by less than 5%.

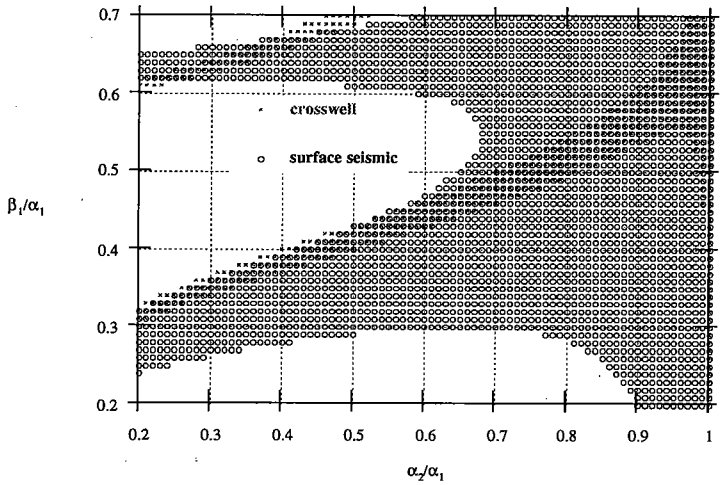

Figure 13: Shaded areas denote values of β_1/α_1 and α_2/α_1 such that error of average angular *PP* from normal incidence *PP* yields a less than 5% error in α_2 from the actual value (Appendix B).

Figures 12 and 13 are shaded mostly on the right. This region corresponds to near equal *P*-wave velocities. With α_1 near α_2, acoustic impedance is small for all incident angles and so reflectivity is as well. Therefore, even if the averaged *PP* differs from the normal incidence *PP* by a large percentage, velocity inversion will still be accurate since *PP* is added to and subtracted from unity in Eqn. (5). This observation makes sense because if compressional velocities are nearly equal, then mathematical interpolation that relates one *P*-wave velocity to the other should be more stable than if the velocities were very different.

The crosswell region on the figures is smaller than the surface seismic region, because the latter is averaged from angles closer to normal incidence, therefore the corresponding reflectivities and estimated velocities are more accurate.

Other Reflectivity Types

I focus on *PP* average reflectivities not only because of their wider use in the field, but also because other average reflectivities and reflectivity zeroes do not provide a useful inversion. Although the equation for *SH*-wave reflectivity,

$$SH = \frac{\rho_2\beta_2 \cos j_2 - \rho_1\beta_1 \cos j_1}{\rho_2\beta_2 \cos j_2 + \rho_1\beta_1 \cos j_1} \qquad (6)$$

is much like Eqn. (4), one can not invert for lower half-space shear velocity using reflectivities from higher angles in the equation for normal incidence. The residuals between the normal incidence *SH* and the angular averages of *SH* are too high to provide a plausible inversion, and *SH* is only near zero at normal incidence, which is trivial.

Attempts at linking *PP* and *SV*-wave reflectivity zeroes with rock properties were also fruitless. The number of velocity and density ratios involved in their calculation is too great to define discrete, meaningful relationships between their values and the behavior of zeroes.

Simple zero incidence reflectivity/velocity èquations, like Eqn. (4), do not exist for converted waves and *SV*- to *SV*-wave reflections. Converted wave reflectivities, *PS* and *SP*, can not be used for inversion in the above manner, because they are always zero perpendicular to the interface. Little can be learned from the behavior of *PS* and *SP* zeroes, because they depend upon too many variables simultaneously.

DISCUSSION

Because of the interdependency of the input ratios in the Zoeppritz equations, studying the effect on reflectivity of changing a single ratio is a wasted effort. However, a multi-variable examination provides some insight toward devising an inversion scheme from average reflectivity. I can use the two variable velocity inversion method as a self-consistency check, by solving for α_2 and β_2 from *PP*, α_1, and β_1, and by comparing with other velocity estimation techniques such as sonic logs or traveltimes.

If I know upper half-space velocities, I can read off a corresponding range of a values from the error envelope and estimate a range for $\alpha_2 = a \times \alpha_1$. I can then solve for α_2 directly from the *PP* velocity inversion formula and compare the two methods to see if the method works for that particular layering scheme.

A possible application of this method is as an estimate of degree of inhomogeneity, anisotropy, and viscoelasticity. If I have upper half-space velocities that fall within a small error envelope, I can then make confident estimates of lower half-space velocities, under the same assumptions from which the original Zoeppritz equations were derived. The difference between my estimates of α_2 and β_2 and those calculated from a sonic log, traveltime, or some other means might be able to give me an idea of how much these assumptions of isotropy, homogeneity, and elasticity are violated in the media.

Figure 12, which shows the velocity ratio regions that yield an inversion within 5% of the true velocity, demonstrates the importance of shear wave velocity information for making an inversion at a common depth point. Estimates of α_2 will be often be incorrect if large offset reflectivity (averaged or discrete angles) is substituted for normal incidence reflectivity.

Check of Velocity Inversion Error

I use the synthetic layering numbers and McElroy log numbers to check the error in velocity estimation associated with them. For the synthetic case the estimated *PP* averaged from typical crosswell incidence angles results in an α_2 value that is about 5 percent too low, while for the McElroy simulation, the estimated velocity is within 1% of the original value. These two layering models do not demonstrate serious problems associated with the use of large offset *PP*, possibly because α_1 and α_2 are about the same. From Figure 10, one can see that for α_2/α_1 ratios near unity, velocity error is minimal.

The assumption I make to arrive at Eqn. (5), namely $\rho_1=\rho_2$, is not normally appropriate. If density is not constant, then Eqn. (5) becomes

$$\alpha_2 = -\alpha_1\left(\frac{\rho_1}{\rho_2}\right)\left(\frac{PP+1}{PP-1}\right). \qquad (7)$$

The density ratio sometimes acts as a correctional factor, as in the synthetic case. Using the density factor, estimated α_2 is only 1% above its true value. Using density,

though, can lead to problems in other situations. Another two layer model, approximating a carbonate over a sand, with properties,

upper layer (1) - density = 2.80 g/cm3 $\alpha = 6.20$ km/s $\beta = 3.50$ km/s
lower layer (2) - density = 2.20 g/cm3 $\alpha = 4.10$ km/s $\beta = 2.50$ km/s

actually works better if densities are assumed to be equal. Using Eqn. (5) to solve for α_2 from *PP* averaged from typical crosswell angles yields a value of 4.09 km/s, an excellent result. Conversely, if Eqn. (7) is used, the value is 5.21 km/s. Therefore, contrary to intuition, accounting for the density differential across the interface is not always more accurate.

There are three cases to consider when trying to calculate lower compressional velocity in a system of two flat, elastic layers. If α_1 is approximately equal to α_2, then, as I have shown, inversion using *PP* reflectivity averages is reliable, because reflectivities are small. If α_1 is less than α_2, then α_2 can be solved using the travel times from head waves through the lower medium. Finally, if α_1 is appreciably greater than α_2, head waves do not exist so reflectivity analysis would be an option. However, if the average reflectivity is not near zero or the normal reflectivity value, then caution must be used to avoid errors when analytically solving for α_2.

LIQUID-SOLID INTERFACE

A *P*-wave incident on a liquid-solid boundary from the liquid will, except at normal or grazing incidence, yield a reflected *P*-wave, a transmitted *P*-wave, and a transmitted *S*-wave [Bourbie 1982] (Figure 14). This seismic wave geometry corresponds to marine surveys in which shots emanate from the water and reflect off the sea floor, or to the non-destructive testing of a material immersed in a liquid using scanning beams. The reflectivity varies according to the angle of incidence of the wave, the elastic wave velocities of the materials, and their relative densities (Appendix C).

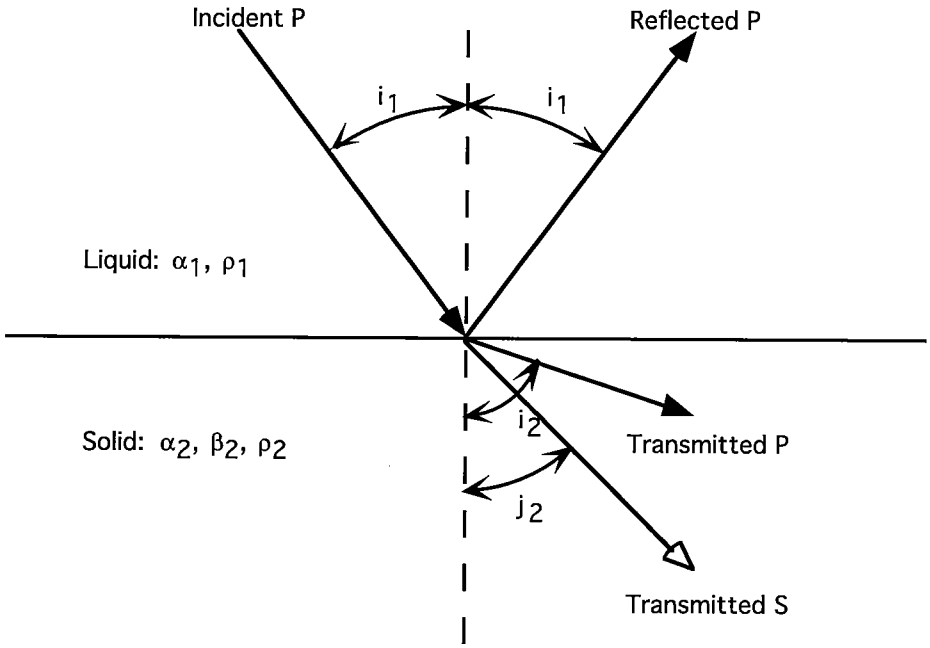

Figure 14: Reflection, transmission, and conversion of a *P*-wave incident on a liquid-solid interface ($\alpha_2 > \beta_2 > \alpha_1$).

Use of Maximum PP

Reflectivity values can indicate, in a non-intrusive manner, some properties of the solid. Although an examination of individual *PP* values does not provide much help in developing a relationship between reflectivity and material properties, maximum *PP* values do show promise. Because there are no *S*-waves in the liquid, the *b* value, β_1/α_1, is not relevant for this type of interface. Remaining are the ratios that concern density, α_2, and β_2. Given the α_2/α_1 values of 2, 4, and 6, the following three figures depict those points where *PP* reflectivity is a maximum for pre-critical incident angles.

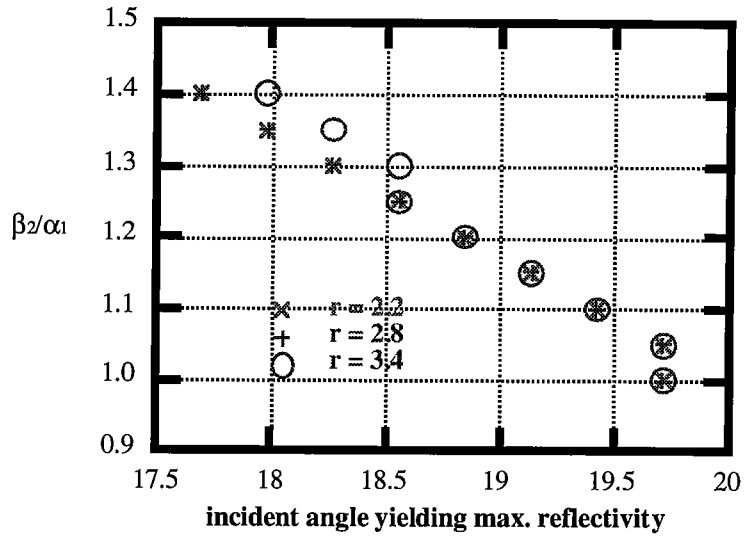

Figure 15: Points indicate the *P*-wave incident angle (on the solid from the liquid) and the ratio β_2/α_1 that yield the highest *PP* reflectivity. For this case, $\alpha_2/\alpha_1 = 2$.

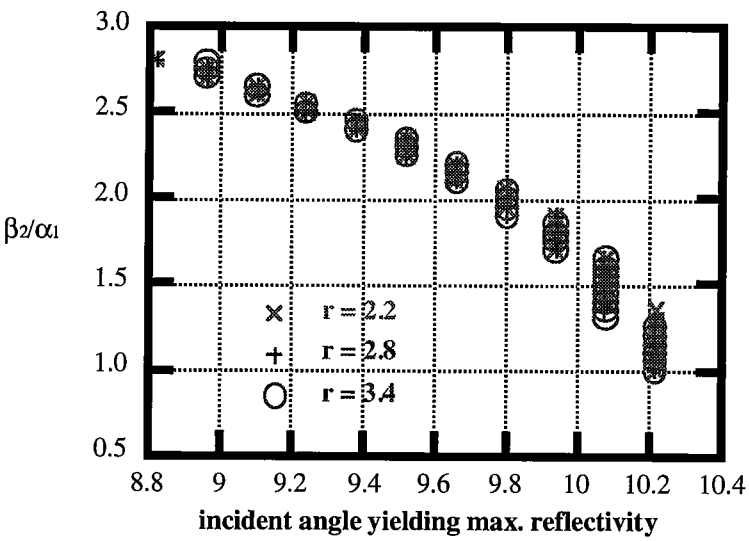

Figure 16: Points indicate the *P*-wave incident angle and the ratio β_2/α_1 that yield the highest *PP* reflectivity. For this case, $\alpha_2/\alpha_1 = 4$.

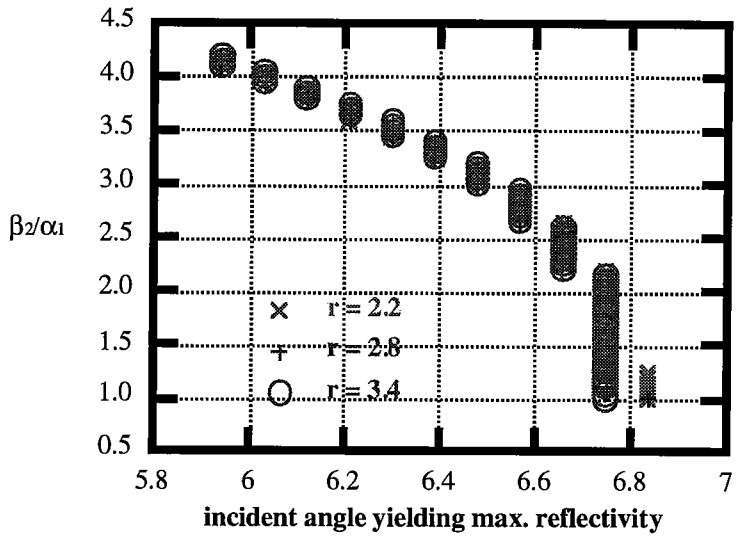

Figure 17: Points indicate the *P*-wave incident angle and the ratio β_2/α_1 that yield the highest *PP* reflectivity. For this case, $\alpha_2/\alpha_1 = 6$.

DISCUSSION

Points corresponding to different densities lie either on top of each other or so close together that distinguishing them individually is very difficult. Therefore, Figures 15-17 clearly show that r, the ratio of the solid density to the liquid density, has little bearing on the relationship between β_2/α_1 and the incident angle which yields the largest amplitude reflected *P*-wave. The vertical axis of β_2/α_1 increases as α_2/α_1 increases, because if α_2 is higher, then β_2, which must be less than the product of $(.5)^{1/2}$ and α_2 for elastic waves, can be higher. The range of pre-critical angles yielding the maximum reflection coefficient decreases with increasing α_2/α_1, because the critical angle decreases sharply.

The relationships illustrated in Figures 15-17 could be useful in determining elastic properties of solids. From preliminary lab measurements one can find values for liquid and solid densities and α_1. Then, measuring reflected amplitudes from the solid-liquid interface, that angle which produces maximum reflectivity can be recorded. The critical angle can be found as well. These angles provide values for β_2/α_1 and α_2/α_1, respectively, which, in turn, give values for elastic velocities within the solid. Once these are known, calculation of elastic constants such as bulk or shear modulus is elementary.

FREE-SOLID INTERFACE

At the interface between a solid half-space and a vacuum, a *P*-wave yields, except at normal incidence, a reflected *P*-wave and a reflected *SV*-wave [Aki and Richards 1982] (Figure 18). This seismic wave geometry usually describes earthquake waves that travel from the hypocenter to the surface and reflect off it. The free-solid interface is also applicable to crosswell though. Waves originating in one well bounce at different angles off the free surface and are detected by receivers in the other well. The reflectivity of the two scattered waves is their amplitude divided by that of the incident wave. The reflectivity varies according to the angle of incidence of the wave and the elastic wave velocities of the solid (Appendix D).

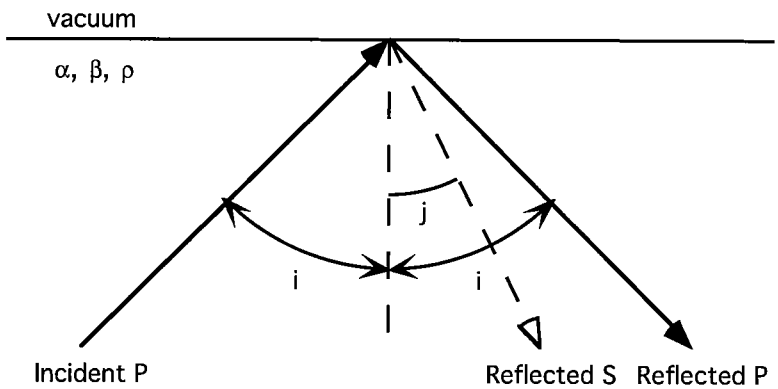

Figure 18: Reflection and conversion of a *P*-wave incident on a free-solid interface [Ewing *et al.* 1957].

Examining the relationship between incidence angle and elastic velocity ratios can provide more than just the solution to a mathematical curiosity. This relationship could be used in materials studies and sonde calibration. In particular, those angles where reflectivity is zero yield information on velocity properties of the solid.

Zero Reflectivity

Because waves cannot transmit through the interface, PP reflectivity is only a function of the angle i and the quantity β/α. If PP is equal to zero, which can be

recognized on seismograms by changes in polarity, then a given incidence angle determines a solid velocity ratio (Appendix D).

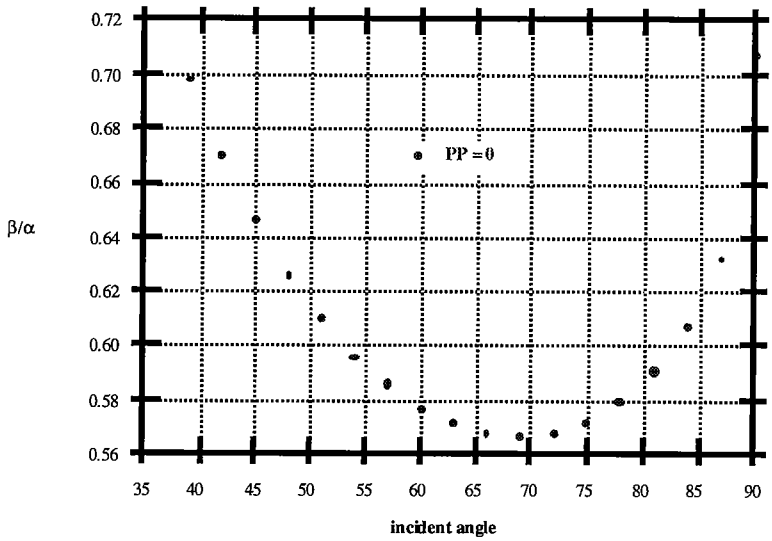

Figure 19: If *PP = 0*, then for a known angle of incidence, a corresponding velocity ratio of the solid can be found. The minimum of the scatter plot is at about 69 degrees, (β/α)=.565.

DISCUSSION

Figure 19 also describes the relationship between i and β/α for incident/reflected *SV*-waves [Aki and Richards 1982]. Reflectivities for converted waves, *PS* and *SP*, equal zero only at normal incidence and grazing incidence (i = 90 degrees). *SH*-wave reflectivity is also not a useful quantity; no wave conversions or transmissions take place so reflectivity should be independent of solid properties. Previously, I did not examine reflectivity zeroes for the solid/solid or liquid/solid cases as I did here, because the number of interdependent velocity and density ratios made finding a relationship such as Eqn. (D3) prohibitive.

A few applications of the i to β/α relationship might exist. Although this section concerns waves incident on the interface from within the solid, if a conjugate relationship exists for those impinging from the other side, then that function could provide a means of non-destructive testing using transducers at the interface. Figure 19 might also have applicability as a check on sonic log measurements. Finally, since the reflectivity equations used in this study assume isotropy, homogeneity, and a flat, elastic interface,

measured residuals from predicted β/α values indicate qualitatively the degree to which those assumptions have failed.

ANELASTICITY

If the materials through which the incident and scattered waves propagate are modeled as anelastic instead of elastic, much of the physics is altered, which affects calculations of reflectivity. Borcherdt (1982) examined the interactions of waves in linear viscoelastic media, at anelastic interfaces. There are a few similarities with the elastic cases, and several differences. As in the elastic case, *P*-waves only convert to *SV*-waves and vice versa as long as the waves are all in the same plane perpendicular to the interface; also, homogeneous waves incident at pre-critical angles will reflect homogeneous waves at the same angle [Borcherdt 1986]. However, Borcherdt (1986) found that transmitted waves will be inhomogeneous for all incident angles, pre- and post-critical, except normal incidence (Figure 20). Intrinsic absorption at a viscoelastic interface causes several other effects not predicted by elasticity theory:

i) phase velocity, indicated by the propagation vector, and energy velocity, indicated by the attenuation vector, propagate with different speeds and directions (Figure 20);

ii) α, β, and the quality factor, Q, which is a measure of attenuation, are all frequency dependent;

iii) phase velocity is dependent on travel path and therefore on incident angle;

iv) energy is transmitted to the lower half-space at post-critical angles due to the interaction of the incident and reflected wavefields and the decrease in the amount of energy transmission is not as abrupt as for the elastic case [Borcherdt 1982,1986].

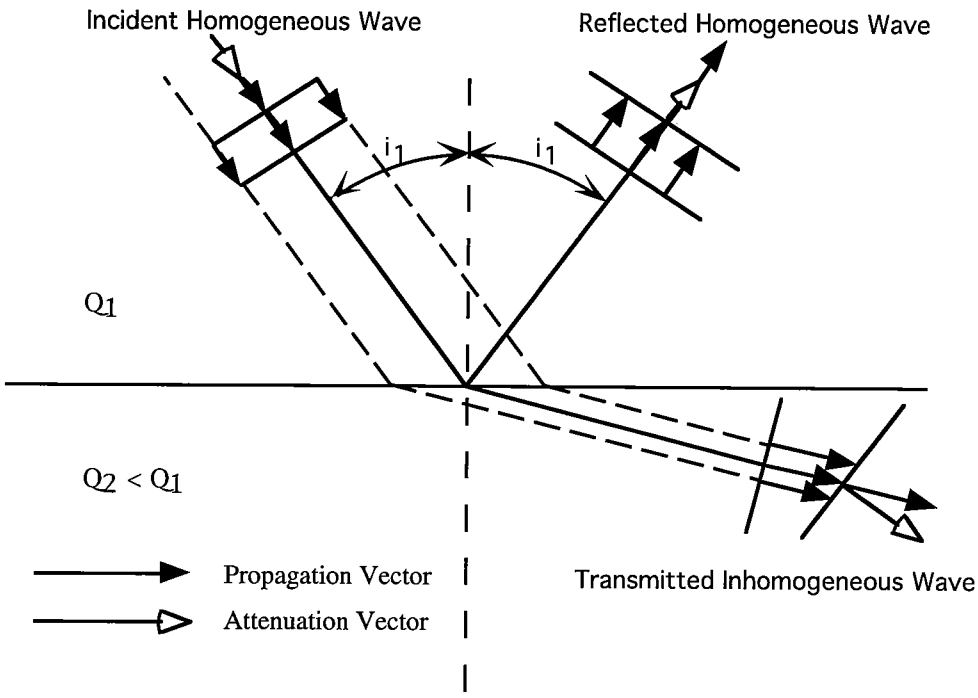

Figure 20: Reflection and transmission of a homogeneous plane wave on an interface between two viscoelastic solids. The propagation vector is perpendicular to planes of constant phase. The attenuation vector is perpendicular to planes of constant amplitude. (Bourbie 1982).

Another effect of anelasticity is particular to a wave within a viscoelastic solid striking a free-surface. Borcherdt (1982) shows that unless $Q_s = Q_p$, an incident *P*-wave will never have a zero reflection coefficient, making the use of Fig.19 problematical.

ACKNOWLEDGMENTS

I would like to thank Jerry Harris and all members of the Seismic Tomography Project for assistance with the conception of this study. I would also like to recognize Mark Van Schaack's invaluable computer support. Funding for this study was provided by Stanford's Seismic Tomography Project Consortium.

REFERENCES

Aki, K. and Richards, P.G., Quantitative Seismology, Theory and Methods, Vol.1. W.H. Freeman and Company, 1980.

Borcherdt, R.D., 1982, Reflection-refraction of general P- and type-I S-waves in elastic and anelastic solids: Geophys. J. R. astr. Soc., 70, p.621-638.

Borcherdt, et al., 1986, Influence of Welded Boundaries in Anelastic Media on Energy Flow, and Characteristics of P, S-I, and S-II Waves: Observational Evidence for Inhomogeneous Body Waves in Low-Loss Solids: J. Geophys. Res., 91, B11, p.11503-11518.

Bourbie, T., Effects of Attenuation on Reflections, PhD Dissertation, Stanford University, 1982.

Ewing, W.M., Jardetzky, W.S., Press, F., Elastic Waves in Layered Media. McGraw-Hill Book Company, Inc., 1957.

Levin, F.K., 1986, When reflection coefficients are zero: Geophysics, 51, p. 736-741.

Tooley, R.D., Spencer, T.W., Sagoci, H.F.,, 1965, Reflection and transmission of plane compressional waves: Geophysics, 30, p. 552-562.

Turcotte, D.L. and Schubert, G., Geodynamics, John Wiley and Sons, Inc., 1982.

APPENDIX A

PP Reflectivity from an Elastic Solid/Solid Interface (Aki and Richards 1982)

The reflection coefficients I use are in terms of displacement amplitudes rather than energy. Displacement amplitude is measured positive in the direction of wave propagation. Seismic receivers generally measure signal only in one direction, vertical or horizontal, but the measured amplitudes can easily be corrected by multiplying by a sine or cosine depending on which component is desired.

Assuming the four possible incident waves, P and S from above and below, and the four scattered waves, the waves' displacement amplitudes are combined with the interface boundary conditions giving a set of four coupled equations. Incident wave displacement amplitudes are $\dot{P}_1$, $\dot{S}_1$, P_2', and S_2'. Scattered wave displacement amplitudes are P_1', S_1', $\dot{P}_2$, and $\dot{S}_2$. The boundary conditions are continuity of displacement and traction in both the parallel and perpendicular directions. The coupled equations are

$$\sin i_1(\dot{P}_1 + P_1') + \cos j_1(\dot{S}_1 + S_1') = \sin i_2(\dot{P}_2 + P_2') + \cos j_2(\dot{S}_2 + S_2'),$$

$$\cos i_1(\dot{P}_1 - P_1') - \sin j_1(\dot{S}_1 - S_1') = \cos i_2(\dot{P}_2 - P_2') - \sin j_2(\dot{S}_2 - S_2'),$$

$$2\rho_1\beta_1^2 p\cos i_1(\grave{P}_1 - P_1') + \rho_1\beta_1\left(1-2\beta_1^2p^2\right)(\grave{S}_1 - S_1') = 2\rho_2\beta_2^2 p\cos i_2(\grave{P}_2 - P_2') + \rho_2\beta_2\left(1-2\beta_2^2p^2\right)(\grave{S}_2 - S_2'),$$

$$\rho_1\alpha_1\left(1-2\beta_1^2p^2\right)(\grave{P}_1 + P_1') - 2\rho_1\beta_1^2 p\cos j_1(\grave{S}_1 + S_1') = \rho_2\alpha_2\left(1-2\beta_2^2p^2\right)(\grave{P}_2 + P_2') - 2\rho_2\beta_2^2 p\cos j_2(\grave{S}_2 + S_2'), \qquad \text{(A1)}$$

where $p = \dfrac{\sin i_1}{\alpha_1} = \dfrac{\sin i_2}{\alpha_2} = \dfrac{\sin j_1}{\beta_1} = \dfrac{\sin j_2}{\beta_2}$, the ray parameter. This is also a mathematical equation describing Snell's Law.

Putting scattered waves on the left and incident waves on the right, we obtain

$$M\begin{pmatrix} P_1' \\ S_1' \\ \grave{P}_2 \\ \grave{S}_2 \end{pmatrix} = N\begin{pmatrix} \grave{P}_1 \\ \grave{S}_1 \\ P_2' \\ S_2' \end{pmatrix}. \qquad \text{(A2)}$$

The complete scattering matrix becomes $M^{-1}N = \begin{pmatrix} \grave{P}P' & \grave{S}P' & P'P' & S'P' \\ \grave{P}S' & \grave{S}S' & P'S' & S'S' \\ \grave{P}\hat{P} & \grave{S}\hat{P} & P\hat{P} & S\hat{P} \\ \grave{P}\hat{S} & \grave{S}\hat{S} & P\hat{S} & S\hat{S} \end{pmatrix}$ (A3)

We are only concerned with the top left term:

$$\grave{P}P' = \frac{\left(B\dfrac{\cos i_1}{\alpha_1} - C\dfrac{\cos i_2}{\alpha_2}\right)F - \left(A + D\dfrac{\cos i_1}{\alpha_1}\dfrac{\cos j_2}{\beta_2}\right)Hp^2}{EF + GHp^2} \qquad \text{(A4)}$$

where

$$\mathrm{A} = \rho_2\left(1-2\beta_2{}^2\mathrm{p}^2\right) - \rho_1\left(1-2\beta_1{}^2\mathrm{p}^2\right),$$
$$\mathrm{B} = \rho_2\left(1-2\beta_2{}^2\mathrm{p}^2\right) + 2\rho_1\beta_1{}^2\mathrm{p}^2,$$
$$\mathrm{C} = \rho_1\left(1-2\beta_1{}^2\mathrm{p}^2\right) + 2\rho_2\beta_2{}^2\mathrm{p}^2,$$
$$\mathrm{D} = 2\left(\rho_2\beta_2{}^2 - \rho_1\beta_1{}^2\right),$$
$$\mathrm{E} = \mathrm{B}\frac{\cos \mathrm{i}_1}{\alpha_1} + \mathrm{C}\frac{\cos \mathrm{i}_2}{\alpha_2},$$
$$\mathrm{F} = \mathrm{B}\frac{\cos \mathrm{j}_1}{\beta_1} + \mathrm{C}\frac{\cos \mathrm{j}_2}{\beta_2},$$

$$G = A - D\frac{\cos i_1}{\alpha_1}\frac{\cos j_2}{\beta_2},$$
$$H = A - D\frac{\cos i_2}{\alpha_2}\frac{\cos j_1}{\beta_1},$$

APPENDIX B

Solving for Error Limitation of α_2 from Error of *PP*

If the two solid half-spaces have equal density, then for normal incidence,

$$\alpha_2 = -\alpha_1\left(\frac{PP+1}{PP-1}\right). \tag{B1}$$

With error in angularly averaged *PP* from normal incidence *PP*, this becomes

$$\alpha_2 = -\alpha_1\left(\frac{PP+\Delta+1}{PP+\Delta-1}\right). \tag{B2}$$

Rearranging,

$$\frac{\Delta}{PP} = \frac{E\left(\frac{1}{PP} - PP\right)}{E(PP+1)+2} \tag{B3}$$

equals the percentage error of *PP*, where E is the percent allowable error of α_2.

Now if $E << \frac{2}{PP+1}$,

$$\frac{\Delta}{PP} = \frac{E\left(1-PP^2\right)}{2PP}, \tag{B4}$$

which is the expression I used to construct Figure 11.

APPENDIX C

PP Reflectivity from an Elastic Liquid/Solid Interface (Bourbie, 1982)

Starting with *P*- and *S*-wave potentials for incident and scattered waves,

$$\Phi_i = A_i \exp\left[ik_{\alpha_1}\left(x\sin i_1 + z\cos i_1\right) - i\omega t\right]$$
$$\Phi_r = A_r \exp\left[ik_{\alpha_1}\left(x\sin i_1 - z\cos i_1\right) - i\omega t\right]$$
$$\Phi_t = A_t \exp\left[ik_{\alpha_2}\left(x\sin i_2 + z\cos i_2\right) - i\omega t\right]$$
$$\psi_t = B_t \exp\left[ik_{\beta_2}\left(x\sin j_2 + z\cos j_2\right) - i\omega t\right], \tag{C1}$$

$$k_\nu = \frac{\omega}{\nu},$$

and combining with boundary conditions of displacement,

$$u_{1_z} = u_{2_z}, \tag{C2}$$

and stress,

$$\begin{aligned} \sigma'_{zx} &= 0 \\ \sigma_{1zz} &= \sigma_{2zz}. \end{aligned} \tag{C3}$$

yields the expression for PP reflectivity from an incident P-wave on a liquid-solid interface:

$$PP = \frac{\rho_2\alpha_2 \cos i_1 \left\{ \left(1-2\sin^2 j_2\right)^2 + \frac{4\beta_2^3}{\alpha_1^2\alpha_2} \sin^2 i_1 \cos i_2 \cos j_2 \right\} - \rho_1\alpha_1 \cos i_2}{\rho_2\alpha_2 \cos i_1 \left\{ \left(1-2\sin^2 i_2\right)^2 + \frac{4\beta_2^3}{\alpha_1^2\alpha_2} \sin^2 i_1 \cos i_2 \cos j_2 \right\} + \rho_1\alpha_1 \cos i_2}. \tag{C4}$$

APPENDIX D

Derivation of Incidence Angle/Velocity Ratio Relationship for a Vacuum/Solid Interface

The boundary conditions for the free surface/solid interface are discontinuity of both displacement and traction. Also, no waves can propagate in the vacuum, and, of course, the vacuum has no density. Combining these conditions with the wave potentials,

$$\begin{aligned} \frac{\partial\psi_x}{\partial x} + \frac{\partial\psi_z}{\partial z} &= 0 \\ \frac{\partial\psi_x}{\partial z} - \frac{\partial\psi_z}{\partial x} &= 0, \end{aligned} \tag{D1}$$

reflectivity can be solved for in terms of the amplitude of the reflected wave divided by the amplitude of the incident wave.

$$PP = \frac{-\left(\frac{1}{\beta^2} - 2p^2\right)^2 + 4p^2 \frac{\cos i}{\alpha} \frac{\cos j}{\beta}}{+\left(\frac{1}{\beta^2} - 2p^2\right)^2 + 4p^2 \frac{\cos i}{\alpha} \frac{\cos j}{\beta}}, \text{(Aki \& Richards p.140)} \tag{D2}$$

where $p = \frac{\sin i}{Vp} = \frac{\sin j}{Vs}$. (D3)

If PP is set to zero then the following relationship results:

$$b^8 + \left(\frac{-1}{\sin^2 i} - 1\right)b^6 + \left(\frac{1.5}{\sin^2 i}\right)b^4 + \left(\frac{-.5}{\sin^4 i}\right)b^2 + \left(\frac{1}{16\sin^6 i}\right) = 0, \tag{D4}$$

where $b = \frac{\beta}{\alpha}$.